



HAL
open science

Dendritic diameter influences the rate and magnitude of hippocampal cAMP and PKA transients during β -adrenergic receptor activation

Vincent Luczak, Kim T. Blackwell, Ted Abel, Jean-Antoine Girault, Nicolas Gervasi

► To cite this version:

Vincent Luczak, Kim T. Blackwell, Ted Abel, Jean-Antoine Girault, Nicolas Gervasi. Dendritic diameter influences the rate and magnitude of hippocampal cAMP and PKA transients during β -adrenergic receptor activation. *Neurobiology of Learning and Memory*, 2017, 138, pp.10-20. 10.1016/j.nlm.2016.08.006 . hal-01514938

HAL Id: hal-01514938

<https://hal.sorbonne-universite.fr/hal-01514938>

Submitted on 26 Apr 2017

HAL is a multi-disciplinary open access archive for the deposit and dissemination of scientific research documents, whether they are published or not. The documents may come from teaching and research institutions in France or abroad, or from public or private research centers.

L'archive ouverte pluridisciplinaire **HAL**, est destinée au dépôt et à la diffusion de documents scientifiques de niveau recherche, publiés ou non, émanant des établissements d'enseignement et de recherche français ou étrangers, des laboratoires publics ou privés.

Title. Dendritic diameter influences the rate and magnitude of hippocampal cAMP transients during β -adrenergic receptor activation

Authors. Vincent Luczak¹, Kim T. Blackwell², Ted Abel¹, Jean-Antoine Girault^{3,4,5} & Nicolas Gervasi^{3,4,5}

Running title: Dendritic diameter influences cAMP transients

¹Department of Biology, School of Arts and Sciences, University of Pennsylvania, Philadelphia, PA, USA.

²George Mason University, The Krasnow Institute for Advanced Studies, Fairfax, Virginia, USA.

³INSERM, UMR-S 839, Paris France.

⁴Université Pierre et Marie Curie (UPMC, Paris 6), Sorbonne Universités, Paris, France.

⁵Institut du Fer à Moulin, Paris, France.

Abstract

In the hippocampus, cyclic-adenosine monophosphate (cAMP) and protein kinase-A (PKA) represent a critical signaling cascade required for long-lasting forms of synaptic plasticity, learning and memory. Plasticity and memory are known to occur following pathway-specific changes in synaptic strength that are thought to result from spatially and temporally coordinated intracellular signaling events. To better understand how cAMP and PKA dynamically operate within the structural complexity of hippocampal neurons, we used live-two photon imaging and genetically-encoded fluorescent biosensors to monitor cAMP levels or PKA activity in CA1 neurons of acute hippocampal slices. Stimulation of β -adrenergic receptors (isoproterenol) or combined activation of adenylyl cyclase (forskolin) and inhibition of phosphodiesterases (IBMX) produced cAMP transients with greater amplitude and rapid on rates in intermediate and distal dendrites compared to soma and proximal dendrites. However, isoproterenol produced greater PKA activity in soma and proximal dendrites compared to intermediate and distal dendrites, but the on rate of PKA activity did not differ by compartment. Computational models show that adenylyl cyclase density increases with compartment diameter and produces rapid and intense cAMP transients in small compartments, whereas phosphatase enrichment in small compartments produces greater PKA activity in large compartments. Together, imaging results and computational models determine that compartmental diameter interacts with rate-limiting components like adenylyl cyclase, phosphodiesterases and protein phosphatases to shape the spatial or temporal components of cAMP and PKA in CA1 neurons and suggests that cAMP greatly impacts signaling in intermediate and distal dendrites, whereas PKA signaling mainly affects soma and proximal dendrites.

1. Introduction

In the hippocampus, long-term potentiation (LTP) and long-term memory (LTM) occur through changes in synaptic plasticity and neuronal excitability. Hippocampal dendrites integrate numerous excitatory and modulatory inputs through morphological and biophysical characteristics that influence excitability, current flow and posttranslational modifications (Spruston, 2008). Dendritic morphology also serves to compartmentalize kinase signaling that differentially produces long-range signals from dendrites to the nucleus that alter epigenetic modifications (Li et al., 2015) or sustain structural plasticity (Zhai et al., 2013). Additionally, computational simulations and biosensor imaging studies find that dendritic geometry can also affect the spread of second-messenger signals within dendrites and influence downstream kinase signaling (Neves et al., 2008, Chay et al., 2015). Although much is known about how dendritic segments can serve as integrators of synaptic inputs, additional molecular studies are needed to determine how dynamic signaling pathways are coordinated with spatial and temporal precision.

Hippocampal LTP and LTM critically rely on production of the second-messenger, cyclic-adenosine 5'-3'-monophosphate (cAMP) and activity of cAMP-dependent protein kinase A (PKA). CyclicAMP levels are tightly regulated through activation and inactivation mechanisms that are thought to operate in close proximity to produce "microdomains" of molecular activity and contribute to synapse-specific plasticity (Harvey et al., 2008; Zaccolo and Pozzan, 2002). Adenylyl cyclases (ACs) synthesize cAMP when stimulated by calcium influx or $G\alpha_s$ subunits released from neuromodulatory G-protein coupled receptors (GPCRs) while phosphodiesterase (PDE) proteins degrade cAMP to restore basal levels. During a cAMP transient, four molecules of cAMP bind to the regulatory subunits of PKA and release diffusible catalytic subunits that phosphorylate and regulate the activity of numerous intracellular targets that participate in plasticity and memory (Turnham and Scott, 2016; Woolfrey and Dell'Acqua, 2015). Increasing

hippocampal cAMP by application of either cell-permeable cAMP analogues, inhibition of PDE4 or direct activation of ACs can enhance several forms of LTM (Barad et al., 1998; Bernabeu et al., 1997; Bourtchouladze et al., 2003; Viola et al., 2000) or LTP (Duffy and Nguyen, 2003; Frey et al., 1993). Similarly, suppression of phosphatase activity by inducible expression of inhibitor-1 (I1) enhances spatial memory (Genoux et al., 2002), but confusingly, bath application of phosphatase inhibitors do not enhance LTP (Woo et al., 2002).

During emotional experiences and heightened states of arousal, the noradrenergic system modulates neuronal activity and promotes LTM by secreting norepinephrine (NE) and increasing cAMP and PKA activity through activation of β -adrenergic receptors (β -ARs) (Cahill et al., 1994; Hu et al., 2007; Sara, 2009). Similarly, exogenous treatment with β -AR agonists can enhance consolidation of LTM in rodents (Izquierdo et al., 1998) or humans (Cahill and Alkire, 2003). However, in hippocampal slices, stimulation of β -ARs with NE or the β -AR agonist isoproterenol (ISO) requires weak synaptic stimulation and NMDA receptor activation to produce an “enhanced” form of pathway-specific LTP (Gelinis et al., 2008; Maity et al., 2015a; Thomas et al., 1996).

To determine how the cAMP/PKA signaling pathway may operate in distinct dendritic compartments, we used live two-photon measurements of genetically encoded fluorescent biosensors to monitor cAMP or PKA activity in hippocampal slices during stimulation of β -ARs. Computational models were then developed to determine how dendritic morphology interacts with activation and inactivation mechanisms to produce molecular constraints that shape dynamic changes in cAMP and PKA activity and compartmentalize signal transduction pathways in hippocampal neurons.

2. Materials and Methods

2.1. Preparation of brain slices and viral transduction

Recombinant Sindbis virus encoding AKAR3 (Allen and Zhang, 2006) or EPAC-sh150 (Polito et al., 2013) were prepared as previously described (Castro et al., 2010). Brains were rapidly isolated from P7-P15, C57BL/6 mice (Janvier; Le Genest Saint Isle, France) and placed in ice-cold “cutting” artificial cerebrospinal fluid (aCSF) containing 110 mM choline Cl, 25 mM NaHCO₃, 1.25 mM NaH₂PO₄, 2.5 mM KCl, 0.5 mM CaCl₂, 7 mM MgCl₂, 25 mM Glucose, 11.6 mM ascorbic acid, 3.1 mM pyruvic acid and saturated with 95% O₂/5% CO₂. Coronal sections (250 μm) were made using a vibrating microtome (Thermo Scientific). Slices were recovered at 30°C for 20 minutes in “standard” aCSF containing 125 mM NaCl, 2.5 mM KCl, 1.25 mM NaH₂PO₄, 25 mM NaHCO₃, 25 mM glucose, 2 mM CaCl₂, 1 mM MgCl₂ (~290 ± 5-10 mOsm) saturated with 95% O₂/5% CO₂ followed by an additional 30 minutes at ~21°C (room temperature). Slices were then transferred to Millicell-CM membranes (Millipore) in culture medium (50% MEM, 50% HBSS, 6.5 g/L glucose, penicillin-streptomycin; Invitrogen), equilibrated for 10 minutes at 35°C with 5% CO₂, and 1 μl Sindbis virus (~5 x 10⁵ particles / slice) was added directly over the hippocampus before overnight incubation at 35°C with 5% CO₂. The following day, slices were transferred to “standard” aCSF saturated with 95% O₂/5% CO₂ at room temperature until used for imaging (<20 hours after viral infection).

2.2. Two-photon slice imaging and drug delivery

On the microscope stage, a nylon/platinum harp stabilized the slice while suspended on nylon mesh to facilitate continuous perfusion over the whole slice at 3 ml/min with “standard” aCSF at 32°C.

Two-photon imaging was performed using an upright Leica TCS MP5 microscope with resonant scanning (8 kHz), a Leica 25X/0.95 HCX IRAPO immersion objective and a tunable Ti:sapphire laser (Coherent Chameleon) with dispersion correction set to 860 nm for CFP excitation. The emission path consisted of an initial 700 nm low-pass filter to remove excess excitation light

(E700 SP, Chroma Technologies), 506 nm dichroic mirror for orthogonal separation of emitted signal, 479/40 CFP emission filter, 542/50 YFP emission filter (FF506-Di01-25x36; FF01-479/40; FF01-542/50; Brightline Filters; Semrock) and two-channel Leica HyD detector for simultaneous acquisition. Due to the high quantum efficiency and low dark noise of the HyD photodetectors, detector gain was typically set at 10-15% with laser power at 1-5%. Z-stack images (16-bit; 512 x 512) were typically acquired every 15 seconds, but in some cases the “default” minimal frame interval was used. The z-step size was 1-2 μm and total stack size was typically 40-90 sections depending on the slice (~40-180 μm).

Concentrated stocks were diluted in standard aCSF saturated with 95% O_2 /5% CO_2 and continuously bubbled during perfusion. Isoproterenol (10 mM; Tocris) was freshly prepared in Milli-Q water. Forskolin (10 mM; Sigma) and IBMX (100 mM; 3,7-Dihydro-1-methyl-3-(2-methylpropyl)-1*H*-purine-2,6-dione; Tocris) were prepared in 100% DMSO.

2.3. Data analysis and image post-acquisition processing

Images were processed in ImageJ by using maximum z-projections followed by translation registration correction to reduce x/y movement. If Sindbis transduction and expression was especially efficient throughout the slice, a z-projection was made using a subset of the whole image stack to reduce mixing signal from multiple cells along the z-axis. However, z-projections were occasionally complicated by movement in the z-axis and were therefore corrected with a custom Matlab script before measurement in ImageJ. After correcting movement in the x/y/z directions, regions of interest (ROIs) were selected for measurement if they could only be measured for the whole experimental timecourse. ROIs were placed around the periphery of the soma to exclude the nuclear compartment and only somata that were reasonably considered to be in stratum pyramidale of hippocampal area CA1 were measured. Proximal dendrites were the region of apical dendrite between the soma and initial dendritic branch, usually <35 μm from

the soma. Intermediate dendrites were between the proximal dendrite and distal dendrites, typically 35-90 μm . Distal dendrites were the most distal dendritic compartment that could be observed and were believed to be connected to neurons in the pyramidal cell layer with a distance 90-150 μm (see Fig. 1A).

After ROI placement, raw CFP and YFP intensity measurements for the entire timecourse were imported into Microsoft Excel. A fluorescence ratio was calculated and for each time point in each ROI series and was normalized to the average baseline ratio for each respective ROI (average of 20 frames before first stimulus). For each ROI, peak amplitudes were determined by finding the maximum point during the stimulus interval (e.g. isoproterenol treatment), and taking the average of 2 points on either side of the max (average of 5 points total). For each ROI, the peak on rate was determined by measuring the maximum slope over 4-5 points of the rising phase and peak off rate was determined by measuring the minimum slope over 10-15 points of the falling phase starting after the peak isoproterenol response.

Statistical analysis was performed in GraphPad Prism. One-way ANOVA followed by Tukey's multiple comparison test was used to identify significant differences in the means of each neuronal compartment. Two-tailed, unpaired t-test was used to compare the mean response in all dendrites to the mean response in somata.

2.4 Computation Modeling

We created a computational model of the βAR and calcium activated signaling pathways in hippocampal CA1 pyramidal neurons using NeuroRD version 3.0 (Jedziewski-Szmek and Blackwell, J Chem Physics, In Press). The morphology of the model represents a thin slice of dendrite: either a 6.5 μm diameter proximal dendrite, or a thinner, 1.5 μm diameter distal dendrite. The morphology is subdivided into two 0.25 μm submembrane voxels and additional 1 μm voxels. In the model, βAR stimulation activates the Gs subtype of GTP binding protein, which activates adenylyl cyclase (AC) types 1 and 5, to produce cAMP. AC1 additionally

requires calcium-bound calmodulin binding for activation. cAMP activates protein kinase A (PKA), which invokes several feedback mechanisms controlling cAMP dynamics. PKA phosphorylates both phosphodiesterase type 4, which enhances its activity, and β AR, which inactivates the receptor. Calbindin and calcineurin are included in the model to maintain physiological levels of calcium and calmodulin. In the model, β AR, G protein, AC and PKA holoenzyme are localized in the submembrane domain and do not diffuse. Cyclic-AMP, the catalytic subunit of PKA, PDE4 and calmodulin diffuse. For one set of simulations, one additional set of molecules was included: inhibitor-1, which is phosphorylated by active PKA and dephosphorylated by calcineurin; protein phosphatase 1, which is inhibited by phosphorylated inhibitor1; and a non-specific PKA phosphoprotein called molecule X. In simulations using this additional set of molecules, protein phosphatase 1 dephosphorylates PDE4 and molecule X. In all cases, phosphorylated PDE4 is used as a read-out of the PKA activity, comparable to the AKAR fluorescence measured in the experiments. All model files needed to run the simulations (or to examine molecule quantities, diffusion constants and reaction rate constants) are available on ModelDB ([accession number XXX](#)).

3. Results

3.1. β -AR stimulation produces cAMP transients with greater rates and amplitudes in intermediate and distal dendrites compared to proximal dendrites and somatic compartments

In the first series of experiments, we explored how cAMP dynamics operate in hippocampal neurons during stimulation of β -ARs. Young hippocampal slices were infected with Sindbis virus encoding the cAMP FRET-based biosensor EPAC-S^{H150}, which consists of a truncated and catalytically inactive version of EPAC1 (Klarenbeek et al., 2011) sandwiched between mTurquoise2 and cp174Citrine (Polito et al., 2013). Cyclic-AMP transients were monitored in CA1 pyramidal neurons in real time using two-photon excitation, ratiometric (F480/F535) microscopy. Up to four compartments were measured in CA1 neurons that included proximal,

intermediate, and distal segments of apical dendrites, and regions of the cell body excluding the nucleus (see Fig. 1A for compartmental breakdown). The general design of these experiments included a 10 minute baseline before a 10 minute treatment with the β -AR agonist isoproterenol (100 nM or 1 μ M) and finally, a 10 minute combined treatment with the adenylyl cyclase activator, forskolin (10 μ M) and the broad-spectrum phosphodiesterase (PDE) inhibitor, IBMX (100 μ M) (Fig. 1B). We initially tested two different concentrations of isoproterenol (100 nM or 1 μ M) and observed a similar trend in cAMP levels with a greater amplitude and rate in dendrites compared to the soma and therefore combined the data from these experiments. Overall, we found that isoproterenol produced the largest amplitude cAMP transients in intermediate ($30.4 \pm 2.5\%$, $n = 21$) and distal dendrites ($22.8 \pm 2.0\%$, $n = 36$) that were significantly greater than proximal dendrites ($18.8 \pm 1.7\%$, $n = 21$) and somata ($14.3 \pm 1.3\%$, $n = 37$). Additionally, the average amplitude of cAMP transients in all dendrites was significantly greater than all somatic compartments during isoproterenol treatment (soma: $14.3 \pm 1.3\%$, $n = 37$ vs. total dendrites: $23.8 \pm 1.3\%$, $n = 78$) (Fig. 1C). During treatment with FSK+IBMX, cAMP amplitudes in intermediate ($58.6 \pm 3.6\%$, $n = 21$) and distal dendrites ($50.4 \pm 3.5\%$, $n = 36$) were still significantly greater than proximal dendrites ($43.4 \pm 2.2\%$, $n = 21$) and somata ($39.6 \pm 1.7\%$, $n = 37$), and the average amplitude of cAMP transients in all dendrites was significantly greater than all somatic compartments (soma: $39.6 \pm 1.7\%$, $n = 37$ vs. total dendrites: $50.7 \pm 2.1\%$, $n = 78$) (Fig. 1C). Calculating the average on rate of cAMP produced with isoproterenol found that intermediate dendrites ($0.77 \pm 0.06 \Delta\text{Ratio\%/second}$, $n = 21$) were significantly greater than proximal dendrites ($0.52 \pm 0.05 \Delta\text{Ratio\%/second}$, $n = 21$) and both intermediate and distal dendrites ($0.70 \pm 0.05 \Delta\text{Ratio\%/second}$, $n = 36$) were greater compared to somatic compartments ($0.36 \pm 0.03 \Delta\text{Ratio\%/second}$, $n = 37$). Overall, the average on rate of cAMP transients was nearly twice the observed rate in somata (soma: $0.36 \pm 0.03 \Delta\text{Ratio\%/second}$, $n = 37$ vs. total dendrites: $0.67 \pm 0.03 \Delta\text{Ratio\%/second}$, $n = 78$) (Fig. 1D). The average on rate of cAMP during endpoint treatment with FSK+IBMX followed the same pattern for the average on

rate with isoproterenol: intermediate ($0.83 \pm 0.06 \Delta\text{Ratio\%/second}$, $n = 21$) and distal dendrites ($0.79 \pm 0.06 \Delta\text{Ratio\%/second}$, $n = 36$) were greater than proximal dendrites ($0.55 \pm 0.04 \Delta\text{Ratio\%/second}$, $n = 21$) and somatic compartments ($0.49 \pm 0.02 \Delta\text{Ratio\%/second}$, $n = 37$) and the average on rate of cAMP in all dendrites was significantly faster compared to somata (soma: $0.49 \pm 0.02 \Delta\text{Ratio\%/second}$, $n = 37$ vs. total dendrites: $0.74 \pm 0.03 \Delta\text{Ratio\%/second}$, $n = 78$) (Fig. 1D).

3.2. β -AR stimulation produces PKA activity with greater amplitude responses in proximal dendrites and somata compared to intermediate and distal dendrites

PKA is a major target of cAMP that plays an important role in regulating neuronal function that contributes to synaptic plasticity and memory. To determine how PKA activity is dynamically regulated during β -AR activation, we used Sindbis virus to express the PKA FRET sensor, AKAR3, which contains a PKA consensus phosphorylation motif and a phospho-binding domain sandwiched between ECFP and cpVenus (Allen and Zhang, 2006). PKA activity was monitored in CA1 neurons of young slices and the FRET ratio was calculated over time (F535/ F480) during stimulation with 1 μM isoproterenol before endpoint treatment with FSK+IBMX (Fig. 2B). The amplitude of PKA activity was significantly larger in somata ($6.6 \pm 0.7\%$, $n = 23$) and proximal dendrites ($6.7 \pm 0.8\%$, $n = 19$) with isoproterenol treatment compared to distal dendrites ($3.9 \pm 0.6\%$, $n = 20$), but there was no significant difference from intermediate ($5.0 \pm 0.4\%$, $n = 40$) or total dendrites. Together, isoproterenol produced a small but significant difference in peak PKA activity between somata and the average dendritic response (soma: $6.6 \pm 0.7\%$, $n = 23$ vs. total dendrites: $5.1 \pm 0.3\%$, $n = 79$) (Fig. 2C). Treatment with FSK+IBMX produced PKA activity in somata ($12.2 \pm 0.8\%$, $n = 23$) and proximal dendrites ($11.2 \pm 1.4\%$, $n = 19$) that was nearly twice the amplitude produced with isoproterenol treatment, and both were significantly greater than peak PKA activity in intermediate ($4.7 \pm 0.5\%$, $n = 40$) and distal dendrites ($4.3 \pm 0.8\%$, $n = 20$). PKA activity in somatic compartments was significantly greater

than the average dendritic response produced with FSK+IBMX (soma: $12.2 \pm 0.8\%$, $n = 23$ vs. total dendrites: $6.2 \pm 0.6\%$, $n = 79$) (Fig. 2B).

During isoproterenol treatment, the rate of PKA activity was not significantly different across neuronal compartments for either the on rate or off rate (Fig. 2D). However, stimulation with FSK+IBMX significantly increased the on rate of PKA activity in proximal dendrites (0.21 ± 0.02 $\Delta\text{Ratio\%/second}$, $n = 19$) compared to distal dendritic segments (0.14 ± 0.01 $\Delta\text{Ratio\%/second}$, $n = 20$) (Fig. 2D).

3.3. Computational models show that an asymmetric density of adenylyl cyclase underlies compartmental differences in cAMP transients and excess PKA subunits do not increase the normalized change in phosphorylated PKA substrates.

To better understand the molecular signaling events producing the compartmental differences in cAMP concentration that we observed during live-imaging experiments, we developed a spatial, stochastic computational model. A $1.5 \mu\text{m}$ width compartment served as a small intermediate or distal dendritic compartment; and a $6.5 \mu\text{m}$ width compartment served as a large proximal dendrite. The resting level of cAMP is determined by a balanced, steady-state reaction between cAMP production by adenylyl cyclase (AC) and cAMP degradation by phosphodiesterase (PDE), and thus initial simulations used basal cAMP concentration as the constraint on the quantity of AC and PDE. These initial simulations found that to achieve a similar level of cAMP in both compartments (identical PDE concentrations), the density of AC needed to be higher in the $6.5 \mu\text{m}$ compartment compared to the $1.5 \mu\text{m}$ compartment. Specifically, to achieve a stable resting level of ~ 100 nM cAMP, AC density was adjusted so that $1.5 \mu\text{m}$ compartments contained $1,700 \text{ pM/m}^2$ and $6.5 \mu\text{m}$ compartments contained $7,200 \text{ pM/m}^2$ (Fig. 3A).

When these tuned models were stimulated with $1 \mu\text{M}$ isoproterenol, the rate and amplitude of cAMP transients were greater in small compartments compared to large compartments (Fig. 3A)

suggesting that an asymmetric distribution of AC density may underlie our observed experimental result (Fig. 1). To verify that AC density, rather than PDE concentration, needs to be asymmetric, we created two additional model variants, each constrained to have ~100 nM basal cAMP, in which the AC density was the same in both compartments and the concentration of PDE (represented by PDE4) was adjusted to stabilize basal cAMP levels. With a high, uniform density of AC ($7,200 \text{ pM/m}^2$) in both small and large compartments, the small compartment required nearly 4 fold more PDE4 (4,420 nM) compared to the large compartment (1,100 nM) to maintain a 100 nM resting level of cAMP (Fig 3B). Similarly, with a low, uniform density of AC ($1,700 \text{ pM/m}^2$) in both small and large compartments, the small compartment required nearly 4 fold less PDE4 (250 nM) compared to the large compartment (1,100 nM) to achieve stable baseline cAMP levels (Fig 3C). Both of these figures show that when AC density is the same in both size compartments, the cAMP transients are similar in both compartments and do not reproduce the experimental observations of larger cAMP transient in the small dendrites. Because the conditions used in Fig. 3A produced cAMP transients that resembled the pattern we observed in imaging experiments, we concluded that a uniform distribution of PDE4 and an asymmetric distribution of adenylyl cyclase may be representative of how cAMP signaling is coordinated *in vivo* and these conditions were used to explore the mechanisms regulating PKA dynamics.

3.4 Computational models show that increased phosphatase concentrations can limit the normalized change in phosphorylated PKA substrates.

Protein kinase-A (PKA) is one of the major effectors regulated by cAMP; thus a greater cAMP signal is predicted to produce a larger PKA signal. Because the live imaging revealed a larger PKA signal in dendritic regions with smaller cAMP signals, we used computational modeling to evaluate several mechanisms that might account for these results. When active, PKA releases diffusible catalytic subunits (PKAcat) that interact with and phosphorylate substrate proteins that

carry the consensus phosphorylation sequence specific for PKA. One possible mechanism is that the small dendritic compartments have a lower concentration of PKA. A second possible mechanism is that small dendritic compartments have a higher concentration of phosphatases that dephosphorylate the AKAR sensor. Protein phosphatases, such as PP1, PP2A or PP2B/calcineurin dephosphorylate substrates phosphorylated by PKA, which serves to maintain steady-state levels of phosphorylated substrates and reset the signaling pathway after receiving a stimulus. A third possible mechanism is that smaller compartments have a greater concentration of substrate proteins which compete with AKAR for the catalytic subunit of PKA (PKAcat). We evaluated PKA activity using two measures: 1. "PKAcat bound + free" represents all PKAcat subunits that are released from PKA regulatory subunits (PKAreg). This measure does not account for phosphatase activity or amount of substrate proteins. 2. Because the AKAR sensor has not been biochemically characterized, we evaluated the phosphorylation of PDE4 to represent PKA activity. This measure is sensitive to phosphatase activity and the amount of competing substrate proteins.

Using our conditions determined by modeling cAMP signaling, which included a uniform distribution of PDE4 and an asymmetric distribution of adenylyl cyclase (Fig. 3A; Section 3.3), we evaluated whether PKA activity would be greater in the large compartment, as observed experimentally. When PKA concentration, PKA substrate concentration and phosphatase concentration is the same in both larger and small compartments, the model shows that activation of the G-protein coupled transmembrane receptor produced a greater amount of PKAcat bound + free in small compartments compared to large compartments (Fig. 3D), and a greater amount of phosphorylated β -ARs (Fig 3E) and PDE4s (Fig 3F), similar to the difference observed with the cAMP response (Fig. 3A). These simulations do not match the experimental results, suggesting that other signaling molecules contribute to the observations.

We tested which of the three mechanisms could account for the experimental results. First, to evaluate whether PKA concentration can explain the experimental observation, we repeated simulations with 3x increase in PKA concentration in the large compartment. Fig 3E shows that simulated values of phosphorylated β -ARs are greater in the large compartment (Fig. 3E) suggesting that PKA concentration can influence the ability to access membrane bound substrates. However, because our imaging experiments used a diffusible PKA substrate (i.e. our AKAR FRET sensor), it is possible that the phosphorylation status of a membrane bound substrate, like β -ARs, may not be representative of the PKA activity measured by our FRET sensor. In addition, the PKA activity is measured as the ratio of stimulated to basal activity, which cannot be calculated for β -ARs in the model because β -AR are not phosphorylated prior to stimulation. Using the normalized phosphorylation status of uniformly distributed PDE4, our model showed that increasing the amount of PKA in large compartments did not increase phosphorylation of PDE4 (Fig. 3F). Together these findings suggest that the concentration of PKA cannot account for the greater PKA activity observed in the soma as compared to the dendrites.

Next, to evaluate the role of phospho-substrate competition or dephosphorylation via phosphatase activity, we added additional components to the model. These components include: an additional PKA substrate, molecule X, which serves as an unidentified PKA substrate that competes with PDE4; dephosphorylation of PDE4 by protein phosphatase 1 (PP1); and inhibitor-1 (I-1) which binds to and inhibits PP1 when phosphorylated by PKA, establishing a positive-feedback mechanism that prolongs the PKA-dependent phosphorylation of substrates. We estimated the affinities of PKA and PP1 for molecule X as similar to those for PDE4.

The quantity of PP1 and molecule X were adjusted to investigate whether a higher phosphatase in the dendrites or greater competition of substrate for PKA could explain the experimental

results. Fig 4A shows that incorporating PP1, I-1 and X into our computational model did not change the cAMP responses significantly: the cAMP transient remained greater in the small compartment compared to the large compartment. The addition of PP1, I-1 and X produced an increase in the total amount of PKAcat bound + free (Fig. 4B) relative to simulations without PP1, I-1 and X (Fig. 3D), but PKA activity remained greater in the small compartment compared to large compartment. Interestingly, simulations with 5 times more X showed a dramatic increase in the level of PKAcat bound + free (Fig. 4B; red traces) which is likely due to excess substrate X interacting with and delaying PKAcat subunits from reuniting with PKAreg subunits to form the inactive PKA holoenzyme. Nonetheless, the greater quantity of molecule X did not lower the phosphorylation of PDE4 relative to baseline for either quantity of PP1, because molecule X affected both the basal and transient phosphorylation level equally. In contrast, if the amount of PP1 was increased from 1.5 to 3.5 μM in small compartments, the amount of pPDE4 was reduced (Fig. 4C). This result was observed for both high and low levels of molecule X. In summary, our simulation results suggest that PP1 levels, and not PKA quantity or competition from other phosphoproteins, may differentially affect PKA signaling in small compartments and may explain the compartmental differences in PKA activity observed in our imaging experiments.

4. Discussion

Here, we used computational modeling and live fluorescent imaging to investigate the molecular constraints shaping the compartmental dynamics of cAMP and PKA activity in hippocampal neurons. Our imaging experiments show that stimulation of β -adrenergic receptors produces cAMP transients with a greater amplitude and faster on rate in small dendrites compared to large compartments like somata. However, the same stimulation protocol produced greater PKA activity in large compartments compared to small dendrites. Computational modeling of cAMP transients found that as neuronal structures increase in size, the density of rate-limiting

components like adenylyl cyclase must also increase, scaling in a manner similar to cable theory (Zador and Koch, 1994). In hippocampal area CA1, the total amount of adenylyl cyclase appears to be enriched in *stratum pyramidale* (Mons et al., 1995), suggesting that AC density increases with compartment size as predicted by our model. Our computational model also relied on a uniform distribution of PDEs between small and large compartments to shape degradation of cAMP transients after GPCR activation. Interestingly, our experimental imaging results show that the off rate of cAMP transients did not differ between somatic or dendritic compartments (Fig 1D), suggesting that PDE activity may be uniformly distributed as predicted in our simulation. Although it is unknown how PDE activity is distributed within neuronal compartments, biosensor imaging, photolysis of caged cAMP compounds and genetic or pharmacological inhibition of PDE isoforms could be used to quantify the activity of various PDE isoforms acting between different neuronal compartments.

In the absence of protein phosphatases, our computational simulations find that PKA activity is proportional to the size of the cAMP transient in a particular dendritic segment (i.e., a large cAMP transient produces a large amplitude PKA response), however when PP1 is included in the model, PKA activity is differentially reduced in small compartments. Although protein phosphatases are known to interact with A-Kinase Anchoring Proteins (AKAPs) (Skroblin et al., 2010), thereby positioning bidirectional regulatory mechanisms (i.e. kinases and phosphatases) in close spatial proximity, it is currently unknown if protein phosphatases are enriched in small dendritic compartments compared to large compartments.

Adrenergic signaling has been implicated in multiple aspects of memory enhancement that include consolidation (Cahill and Alkire, 2003; Izquierdo et al., 1998), retrieval (Murchison et al., 2004; Schutsky et al., 2011), extinction (Berlau and McGaugh, 2006) and reconsolidation (Gazarini et al., 2013). In hippocampal slices, isoproterenol increases the firing frequency of CA1 neurons in a dose-dependent manner that is selective for β 2-adrenergic receptors and

independent of glutamatergic or cholinergic input (Hillman et al., 2005). Similarly, norepinephrine or isoproterenol treatment lowers the threshold for induction of several forms of long-lasting synaptic plasticity (Gelinias and Nguyen, 2005; Winder et al., 1999) and recent studies suggest this enhancement mainly operates through β 2-ARs (Maity et al., 2015b; Qian et al., 2012). The β 2-AR is known to interact with several AKAPs that are thought to act as multiprotein scaffolds that coordinate and spatially compartmentalize signal transduction pathways. Interestingly, disruption of either AKAP150/AKAP5 or Gravin/AKAP12 impairs β -AR mediated forms of synaptic plasticity and long-term memory, but each AKAP seemingly coordinates a unique component of β -AR signaling. For example, in the case of AKAP150 knockouts, AC5 is excluded from the post synaptic density and isoproterenol treated slices fail to enhance phosphorylation of AMPA receptor subunit GluA1 (pS845) (Zhang et al., 2013), a requirement for β -AR LTP (Qian et al., 2012). Conversely, Gravin mutant mice have reduced levels of phosphorylated β 2-AR (pS345, pS346) and pERK following fear conditioning training (Havekes et al., 2012), a mechanism that is attributed to impaired G-protein switching at β 2-ARs from $G\alpha_s$ to $G\alpha_i$ which is thought to facilitate ERK1/2 activation (Daaka et al., 1997). Despite a great amount of work focused on dissecting the molecular mechanisms of β -AR-mediated signaling, many studies fail to address the spatial and temporal gap between biochemical and electrophysiology results. Fortunately, a diverse set of improved FRET sensors exist to begin investigating the spatial and temporal components of signal transduction that occur during synaptic plasticity.

Our imaging experiments show that despite using a uniform bath application of a β -AR agonist, cAMP levels change with different intensities throughout neuronal compartments with small, intermediate and distal dendrites containing the largest and fastest cAMP transients. This result suggests that small dendrites may be most sensitive to modulatory signals that prime postsynaptic mechanisms necessary for long-term potentiation. For example, in hippocampal

slices, isoproterenol or norepinephrine alone increases phosphorylation of postsynaptic targets that are required for long-lasting plasticity, like ion channels (GluA1) (Qian et al., 2012) or translational regulators (rpS6 and eIF4E) (Maity et al., 2015b). In terms of PKA signaling, our imaging results show that bath application of isoproterenol generated a greater amount of PKA activity in large compartments, like the proximal dendrites and soma, suggesting that large compartments offer a greater dynamic range in PKA activity. Because bath application of the AC activator, forskolin, can produce a form of “chemical LTP” (Chavez-Noriega and Stevens, 1992) but isoproterenol or norepinephrine treatment alone does not induce LTP (O’Dell et al., 2015), then the amount of PKA activity we observed during isoproterenol treatment is subthreshold for LTP induction and suggests that large compartments require activation of additional signaling pathways or integration of multiple sources of cAMP to exceed the threshold for LTP induction.

Our computational simulations identify several potential mechanisms regulating the spatial and temporal dynamics of cAMP and PKA signaling in CA1 neurons. In particular, adenylyl cyclase density increases with compartment size to stabilize basal cAMP levels, excess PKA subunits do not alter the normalized phosphorylation status of a PKA substrate and protein phosphatases suppress PKA activity in small compartments. Our imaging experiments identify a clear induction of activation pathways (i.e., GPCRs and ACs) that increase cAMP and PKA activity. The activation phase immediate followed by inactivation mechanisms (i.e., PDEs and PPs) that reduce cAMP and PKA activity, and thereby produce a “peak” in biochemical activity.

Although our computational simulations show clear activation mechanisms as indicated by a rapid increase in cAMP or PKA activity, large compartments display a gradual rise in cAMP that closely follows PDE activity and masks any “peak” in cAMP (Fig 3A, 4A). Simulations that produce a clear “peak” (e.g. Fig. 3A; cAMP transients in 1.5 μm compartments) result from generating cAMP at a rate that greatly exceeds the onset of inactivation mechanisms.

Experimental manipulation of PDE activity could be used to evaluate the temporal interactions between activation and inactivation. For example, during stimulation of β ARs, inhibition of PDEs may produce large amplitude cAMP transients with a broad peak, whereas PDE overexpression or optogenetic activation of PDEs may produce a gradually increasing, low amplitude cAMP transient that rapidly decays. Nevertheless, our computation models suggest that the shape of biochemical transients reflect interactions between activation and inactivation mechanisms and analyzing the shape of transient activity may be useful when using fluorescent FRET sensors to quantify and dissect signal transduction pathways *in situ*.

Overall, our findings identify neuronal compartments that are most sensitive to β -AR signal transduction and we identify potential biochemical regulatory mechanisms that act to offset changes in neuronal morphology to maintain distinct cAMP or PKA-sensitive compartments.

Acknowledgements

This work was supported by NIMH grant R01 MH086415 (TA), NIAAA grant R01 AA018060 (TA and KB), NSF grant 1515458 (TA), NSF grant 1515686 (KB) and Chateaubriand Fellowship (VL). We wish to thank Pierre Vincent for providing the Sindbis EPAC-S^{H150}, Ludovic Tricoire (UPMC, Paris) for the Matlab script to correct z-drift, and members of the Abel lab for helpful discussions in preparing the manuscript. TA is the Brush Family Professor of Biology at the University of Pennsylvania.

Figure Legends

Figure 1. Cyclic-AMP transients in CA1 neurons have a greater rate and amplitude in dendrites compared to soma during β -adrenergic receptor activation.

(A) *Left*: Cartoon of how EPAC-S^{H150} reports cAMP levels by decreasing the FRET response between a CFP and YFP fluorescent protein. *Center*: Classification of neuronal compartments by distance from soma. *Right*: Representative example of cAMP responses in CA1 neurons of brain slices. (B, C and D) Combined data from experiments using 100 nM or 1 μ M isoproterenol. (B) Timecourse, (C) peak amplitudes during isoproterenol ($F_{(3,111)} = 12.62$, $p < 0.0001$), (### $p < 0.001$) or FSK + IBMX application ($F_{(3,111)} = 7.613$, $p < 0.0001$), (### $p = 0.008$), and (D) average rate of cAMP dynamics during isoproterenol ($F_{(3,111)} = 15.99$, $p < 0.0001$), (### $p < 0.001$) or FSK + IBMX application ($F_{(3,111)} = 13.46$, $p < 0.0001$), (### $p < 0.001$). Data are mean \pm SEM. Soma vs dendritic compartments were analyzed by one-way ANOVA with Tukey's Test ($*p < 0.05$, $**p < 0.01$, $***p < 0.001$). Soma vs total dendrites were analyzed by unpaired, two-tailed t -test with p -value as indicated. Scale bars are 40 μ m.

Figure 2. PKA activity in CA1 neurons is greater in soma and proximal dendrites during β -adrenergic receptor activation.

(A) *Left*: Cartoon of how AKAR3 functions as a substrate and reporter of PKA activity. *Right*: Representative example of PKA activity in CA1 neurons of brain slices. (B, C and D) (B) Average timecourse, (C) average peak amplitude of PKA activity during application of 1 μ M isoproterenol ($F_{(3,98)} = 3.837$, $p = 0.0121$) or FSK + IBMX ($F_{(3,98)} = 5.373$, $p < 0.0001$), (### $p < 0.0001$) and (D) average rates of PKA activity during application of 1 μ M isoproterenol or FSK + IBMX ($F_{(3,98)} = 4.371$, $p = 0.0062$). Data are mean \pm SEM. Neuronal compartments were analyzed by one-way ANOVA and Tukey's Test (confidence intervals = $*p < 0.05$, $**p < 0.01$, $***p < 0.001$). Soma vs total dendrites were analyzed by unpaired, two-tailed t -test with p -value as indicated. Image scale bars are 40 μ m.

Figure 3. Computational modeling determines compartment size and adenylyl cyclase density shape cAMP dynamics and PKA activity does not increase with PKA concentration.

(A) Simulations of a small (1.5 μm) and large (6.5 μm) dendritic compartment with a uniform concentration of PDE4 in both compartments and an asymmetric density of adenylyl cyclase (small=1,700 pmol/m^2 ; large= 7,200 pmol/m^2) produced compartmental differences in cAMP transients that resembled cAMP dynamics measured in live-imaging experiments. (B and C) PDE4 concentrations are adjusted to stabilize baseline cAMP in both small and large compartments. Neither a “high” uniform density of adenylyl cyclase (panel B; AC=7,200 pmol/m^2) nor a “low” uniform density (panel C; AC=1,700 pmol/m^2) produced cAMP transients that resembled cAMP dynamics measured during imaging. (D-F) Simulations using the conditions for AC and PDE4 Fig. 3A. (D) cAMP-activated PKA is greater in the small compartment compared to the large compartment. “PKAc Bound + Free” is the total PKA catalytic subunits released from PKA regulatory subunits (i.e., PKAc Bound= PKAc interacting with a phospho-substrate; PKAc Free= PKAc unbound to both PKAreg and phospho-substrate). (E and F) Phosphorylation status of PDE4 as a fraction of total pPDE4 (panel E) or normalized fraction (panel F). The small compartment has more initial and stimulated pPDE4 compared to large compartments and did not resemble PKA activity measured in live-imaging experiments. Increasing the concentration of PKA subunits increased the basal fraction of pPDE4 (panel E), but reduced the peak fractional change (panel F).

Figure 4. Computational modeling determines that protein phosphatase 1 is a potential mechanism suppressing PKA activity in small dendritic compartments and excess PKA substrate does not affect PKA signaling dynamics.

(A-C) The computational model defined in Fig. 3A was modified to include different concentrations of protein phosphatase 1 (PP1) and elevated concentrations of PKA substrate (molecule “X”). (A) cAMP transients were not affected by different concentrations of PP1 or X. (B) PKAc Bound + Free increases with greater concentrations of X but were unaffected by greater PP1. (C) The normalized phosphorylation status of PDE4 was not affected by different concentrations of X, but was reduced with greater concentrations of PP1.

Figure 5. Summary of compartmental differences influencing cAMP and PKA dynamics.

(Left graphs) Interactions between “activation mechanisms” (ACs) and “inactivation mechanisms” (include PDEs and PPs) shape compartmental differences in cAMP and PKA signaling dynamics. *(Right panels)* Illustrations showing that AC density increases with compartment size and PDE concentrations are relatively the same in both small and large compartments. Phosphatase enrichment in small compartments may be a mechanism limiting bulk PKA activity in small dendritic compartments.

References

- Allen, M.D., and Zhang, J. (2006). Subcellular dynamics of protein kinase A activity visualized by FRET-based reporters. *Biochem. Biophys. Res. Commun.* *348*, 716–721.
- Barad, M., Bourtchouladze, R., Winder, D.G., Golan, H., and Kandel, E. (1998). Rolipram, a type IV-specific phosphodiesterase inhibitor, facilitates the establishment of long-lasting long-term potentiation and improves memory. *Proc. Natl. Acad. Sci. U. S. A.* *95*, 15020–15025.
- Berlau, D.J., and McGaugh, J.L. (2006). Enhancement of extinction memory consolidation: the role of the noradrenergic and GABAergic systems within the basolateral amygdala. *Neurobiol. Learn. Mem.* *86*, 123–132.
- Bernabeu, R., Bevilacqua, L., Ardenghi, P., Bromberg, E., Schmitz, P., Bianchin, M., Izquierdo, I., and Medina, J.H. (1997). Involvement of hippocampal cAMP/cAMP-dependent protein kinase signaling pathways in a late memory consolidation phase of aversively motivated learning in rats. *Proc. Natl. Acad. Sci. U. S. A.* *94*, 7041–7046.
- Bourtchouladze, R., Lidge, R., Catapano, R., Stanley, J., Gossweiler, S., Romashko, D., Scott, R., and Tully, T. (2003). A mouse model of Rubinstein-Taybi syndrome: defective long-term memory is ameliorated by inhibitors of phosphodiesterase 4. *Proc. Natl. Acad. Sci. U. S. A.* *100*, 10518–10522.
- Cahill, L., and Alkire, M.T. (2003). Epinephrine enhancement of human memory consolidation: Interaction with arousal at encoding. *Neurobiol. Learn. Mem.* *79*, 194–198.
- Cahill, L., Prins, B., Weber, M., and McGaugh, J.L. (1994). Beta-adrenergic activation and memory for emotional events. *Nature* *371*, 702–704.
- Castro, L.R. V, Gervasi, N., Guiot, E., Cavellini, L., Nikolaev, V.O., Paupardin-Tritsch, D., and Vincent, P. (2010). Type 4 phosphodiesterase plays different integrating roles in different cellular domains in pyramidal cortical neurons. *J. Neurosci.* *30*, 6143–6151.
- Chavez-Noriega, L.E., and Stevens, C.F. (1992). Modulation of synaptic efficacy in field CA1 of the rat hippocampus by forskolin. *Brain Res.* *574*, 85–92.
- Daaka, Y., Luttrell, L.M., and Lefkowitz, R.J. (1997). Switching of the coupling of the beta2-adrenergic receptor to different G proteins by protein kinase A. *Nature* *390*, 88–91.
- Duffy, S.N., and Nguyen, P. V (2003). Postsynaptic application of a peptide inhibitor of cAMP-dependent protein kinase blocks expression of long-lasting synaptic potentiation in hippocampal neurons. *J. Neurosci.* *23*, 1142–1150.
- Frey, U., Huang, Y.Y., and Kandel, E.R. (1993). Effects of cAMP simulate a late stage of LTP in hippocampal CA1 neurons. *Science* *260*, 1661–1664.
- Gazarini, L., Stern, C.A.J., Carobrez, A.P., and Bertoglio, L.J. (2013). Enhanced noradrenergic activity potentiates fear memory consolidation and reconsolidation by differentially recruiting α 1- and β -adrenergic receptors. *Learn. Mem.* *20*, 210–219.
- Gelinas, J.N., and Nguyen, P. V (2005). Beta-adrenergic receptor activation facilitates induction of a protein synthesis-dependent late phase of long-term potentiation. *J. Neurosci.* *25*, 3294–3303.
- Gelinas, J.N., Tenorio, G., Lemon, N., Abel, T., and Nguyen, P. V (2008). Beta-adrenergic receptor activation during distinct patterns of stimulation critically modulates the PKA-

dependence of LTP in the mouse hippocampus. *Learn. Mem.* 15, 281–289.

Genoux, D., Haditsch, U., Knobloch, M., Michalon, A., Storm, D., and Mansuy, I.M. (2002). Protein phosphatase 1 is a molecular constraint on learning and memory. *Nature* 418, 970–975.

Gervasi, N., Hepp, R., Tricoire, L., Zhang, J., Lambolez, B., Paupardin-Tritsch, D., and Vincent, P. (2007). Dynamics of protein kinase A signaling at the membrane, in the cytosol, and in the nucleus of neurons in mouse brain slices. *J. Neurosci.* 27, 2744–2750.

Harvey, C.D., Yasuda, R., Zhong, H., and Svoboda, K. (2008). The spread of Ras activity triggered by activation of a single dendritic spine. *Science* 321, 136–140.

Havekes, R., Canton, D.A., Park, A.J., Huang, T., Nie, T., Day, J.P., Guercio, L.A., Grimes, Q., Luczak, V., Gelman, I.H., et al. (2012). Gravin Orchestrates Protein Kinase A and β 2-Adrenergic Receptor Signaling Critical for Synaptic Plasticity and Memory. *J. Neurosci.* 32, 18137–18149.

Hillman, K.L., Doze, V.A., and Porter, J.E. (2005). Functional characterization of the beta-adrenergic receptor subtypes expressed by CA1 pyramidal cells in the rat hippocampus. *J. Pharmacol. Exp. Ther.* 314, 561–567.

Hu, H., Real, E., Takamiya, K., Kang, M.-G., Ledoux, J., Huganir, R.L., and Malinow, R. (2007). Emotion enhances learning via norepinephrine regulation of AMPA-receptor trafficking. *Cell* 131, 160–173.

Izquierdo, I., Medina, J.H., Izquierdo, L.A., Barros, D.M., de Souza, M.M., and Mello e Souza, T. (1998). Short- and long-term memory are differentially regulated by monoaminergic systems in the rat brain. *Neurobiol. Learn. Mem.* 69, 219–224.

Klarenbeek, J.B., Goedhart, J., Hink, M.A., Gadella, T.W.J., and Jalink, K. (2011). A mTurquoise-based cAMP sensor for both FLIM and ratiometric read-out has improved dynamic range. *PLoS One* 6, e19170.

Li, L., Gervasi, N., and Girault, J.-A. (2015). Dendritic geometry shapes neuronal cAMP signalling to the nucleus. *Nat. Commun.* 6, 6319.

Maity, S., Jarome, T.J., Blair, J., Lubin, F.D., and Nguyen, P. V. (2015a). Norepinephrine goes nuclear: Epigenetic modifications during long-lasting synaptic potentiation triggered by activation of beta-adrenergic receptors. *J. Physiol.*

Maity, S., Rah, S., Sonenberg, N., Gkogkas, C.G., and Nguyen, P. V. (2015b). Norepinephrine triggers metaplasticity of LTP by increasing translation of specific mRNAs. *Learn. Mem.* 22, 499–508.

Mons, N., Harry, A., Dubourg, P., Premont, R.T., Iyengar, R., and Cooper, D.M. (1995). Immunohistochemical localization of adenylyl cyclase in rat brain indicates a highly selective concentration at synapses. *Proc. Natl. Acad. Sci. U. S. A.* 92, 8473–8477.

Murchison, C.F., Zhang, X.-Y., Zhang, W.-P., Ouyang, M., Lee, A., and Thomas, S.A. (2004). A distinct role for norepinephrine in memory retrieval. *Cell* 117, 131–143.

Neves, S.R., Tsokas, P., Sarkar, A., Grace, E.A., Rangamani, P., Taubenfeld, S.M., Alberini, C.M., Schaff, J.C., Blitzer, R.D., Moraru, I.I., et al. (2008). Cell shape and negative links in regulatory motifs together control spatial information flow in signaling networks. *Cell* 133, 666–680.

O'Dell, T.J., Connor, S.A., Guglietta, R., and Nguyen, P. V. (2015). β -Adrenergic receptor signaling and modulation of long-term potentiation in the mammalian hippocampus. *Learn.*

Mem. 22, 461–471.

Polito, M., Klarenbeek, J., Jalink, K., Paupardin-Tritsch, D., Vincent, P., and Castro, L.R. V (2013). The NO/cGMP pathway inhibits transient cAMP signals through the activation of PDE2 in striatal neurons. *Front. Cell. Neurosci.* 7, 211.

Qian, H., Matt, L., Zhang, M., Nguyen, M., Patriarchi, T., Koval, O.M., Anderson, M.E., He, K., Lee, H.-K., and Hell, J.W. (2012). β 2-Adrenergic receptor supports prolonged theta tetanus-induced LTP. *J. Neurophysiol.* 107, 2703–2712.

Sara, S.J. (2009). The locus coeruleus and noradrenergic modulation of cognition. *Nat. Rev. Neurosci.* 10, 211–223.

Schutsky, K., Ouyang, M., Castelino, C.B., Zhang, L., and Thomas, S. a (2011). Stress and glucocorticoids impair memory retrieval via β 2-adrenergic, Gi/o-coupled suppression of cAMP signaling. *J. Neurosci.* 31, 14172–14181.

Skroblin, P., Grossmann, S., Schäfer, G., Rosenthal, W., and Klussmann, E. (2010). Mechanisms of protein kinase A anchoring. *Int. Rev. Cell Mol. Biol.* 283, 235–330.

Spruston, N. (2008). Pyramidal neurons: dendritic structure and synaptic integration. *Nat. Rev. Neurosci.* 9, 206–221.

Thomas, M.J., Moody, T.D., Makhinson, M., and O'Dell, T.J. (1996). Activity-dependent beta-adrenergic modulation of low frequency stimulation induced LTP in the hippocampal CA1 region. *Neuron* 17, 475–482.

Turnham, R.E., and Scott, J.D. (2016). Protein kinase A catalytic subunit isoform PRKACA; History, function and physiology. *Gene* 577, 101–108.

Viola, H., Furman, M., Izquierdo, L. a, Alonso, M., Barros, D.M., de Souza, M.M., Izquierdo, I., and Medina, J.H. (2000). Phosphorylated cAMP response element-binding protein as a molecular marker of memory processing in rat hippocampus: effect of novelty. *J. Neurosci.* 20, RC112.

Winder, D.G., Martin, K.C., Muzzio, I. a, Rohrer, D., Chruscinski, A., Kobilka, B., and Kandel, E.R. (1999). ERK Plays a Regulatory Role in Induction of LTP by Theta Frequency Stimulation and Its Modulation by β -Adrenergic Receptors. *Neuron* 24, 715–726.

Woo, N.H., Abel, T., and Nguyen, P. V (2002). Genetic and pharmacological demonstration of a role for cyclic AMP-dependent protein kinase-mediated suppression of protein phosphatases in gating the expression of late LTP. *Eur. J. Neurosci.* 16, 1871–1876.

Woolfrey, K.M., and Dell'Acqua, M.L. (2015). Coordination of Protein Phosphorylation and Dephosphorylation in Synaptic Plasticity. *J. Biol. Chem.* 290, jbc.R115.657262.

Zaccolo, M., and Pozzan, T. (2002). Discrete microdomains with high concentration of cAMP in stimulated rat neonatal cardiac myocytes. *Science* 295, 1711–1715.

Zador, A., and Koch, C. (1994). Linearized models of calcium dynamics: formal equivalence to the cable equation. *J. Neurosci.* 14, 4705–4715.

Zhai, S., Ark, E.D., Parra-Bueno, P., and Yasuda, R. (2013). Long-distance integration of nuclear ERK signaling triggered by activation of a few dendritic spines. *Science* 342, 1107–1111.

Zhang, M., Patriarchi, T., Stein, I.S., Qian, H., Matt, L., Nguyen, M., Xiang, Y.K., and Hell, J.W. (2013). Adenylyl cyclase anchoring by a kinase anchor protein AKAP5 (AKAP79/150) is

Dendritic diameter influences cAMP and PKA? transients

important for postsynaptic β -adrenergic signaling. J. Biol. Chem. 288, 17918–17931.

Figure 1.

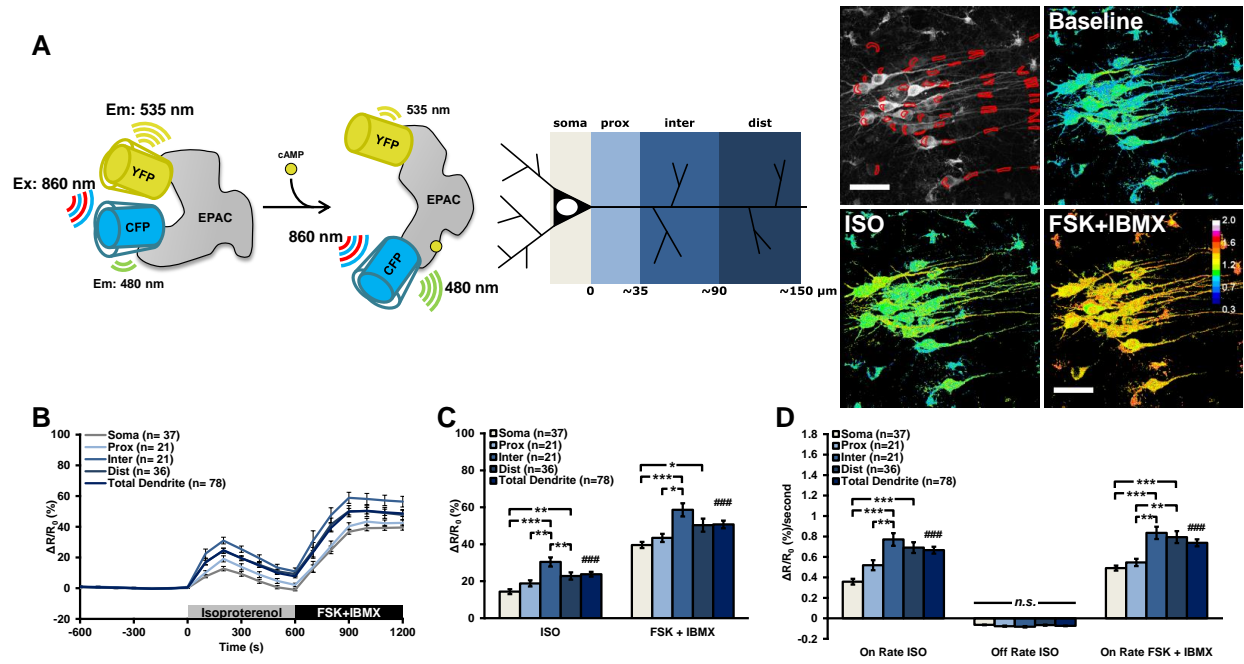
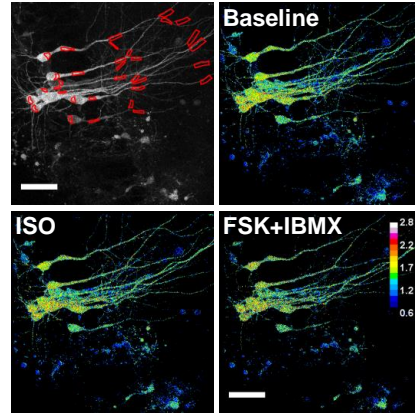
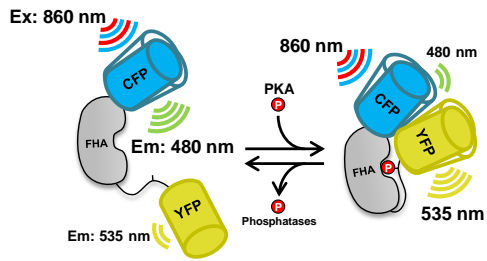
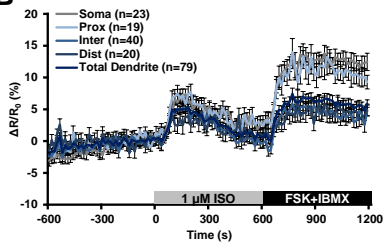


Figure 2.

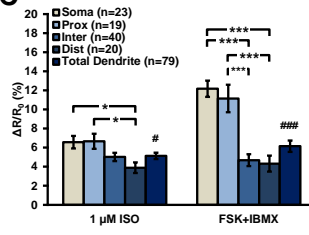
A



B



C



D

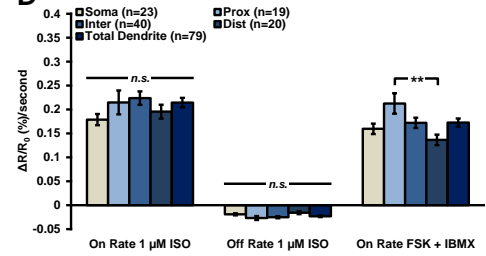


Figure 3.

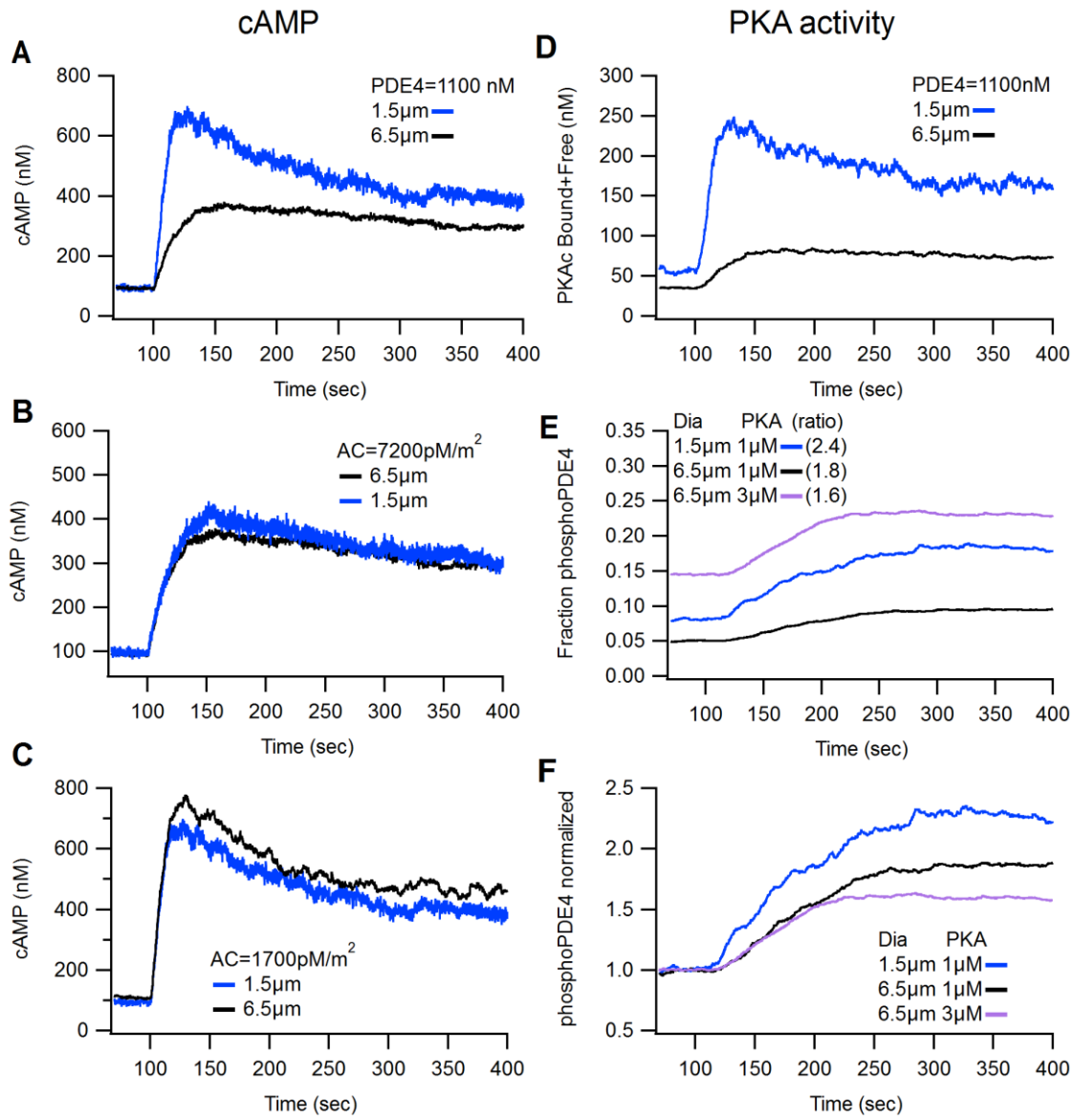


Figure 4.

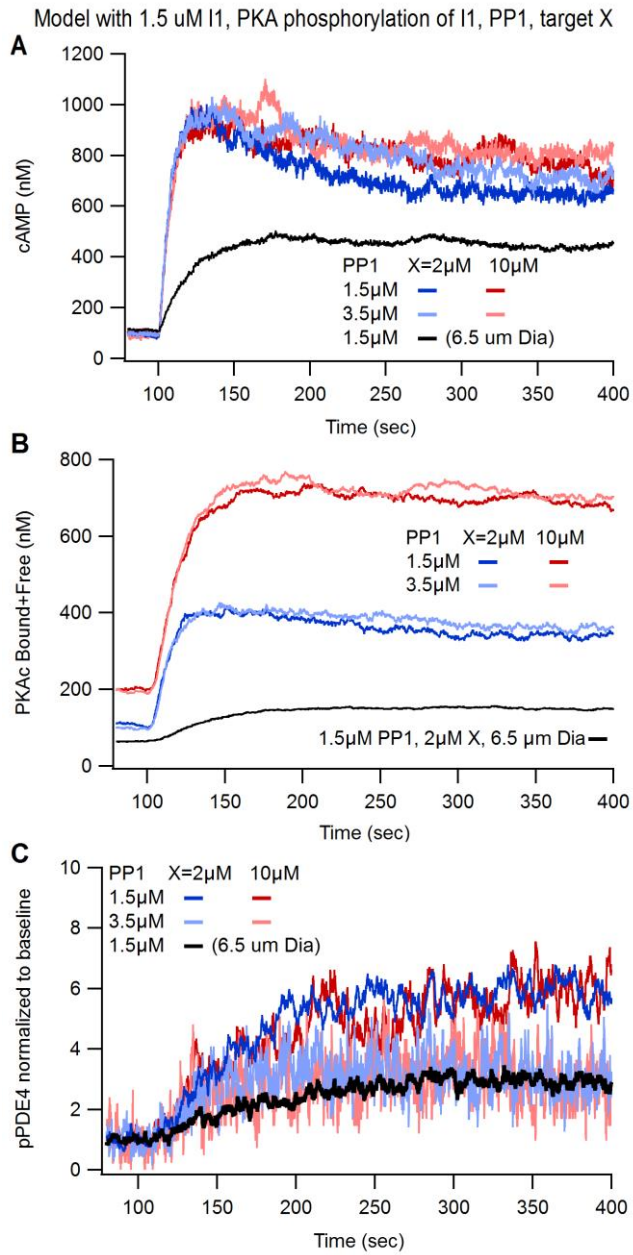


Figure 5.

